Structural Chemistry of "Defect" Cyanometalate Boxes: {Cs⊂[CpCo(CN)₃]₄[Cp*Ru]₃} and {M⊂[Cp*Rh(CN)₃]₄[Cp*Ru]₃} (M = NH₄, Cs)

Matthew L. Kuhlman and Thomas B. Rauchfuss*

Contribution from the Department of Chemistry, University of Illinois at Urbana-Champaign, Urbana, Illinois 61801

Received March 20, 2003; E-mail: rauchfuz@uiuc.edu

Abstract: A series of heptametallic cyanide cages are described; they represent soluble analogues of defect-containing cyanometalate solid-state polymers. Reaction of 0.75 equiv of [Cp*Ru(NCMe)₃]PF₆, Et₄N-[Cp*Rh(CN)₃], and 0.25 equiv of CsOTf in MeCN solution produced {Cs⊂[Cp*Rh(CN)₃]₄[Cp*Ru]₃} (**Cs⊂Rh₄Ru₃**). ¹H and ¹³³Cs NMR measurements show that **Cs⊂Rh₄Ru₃** exists as a single C_s isomer. In contrast, {Cs⊂[CpCo(CN)₃]₄[Cp*Ru]₃} (**Cs⊂Co₄Ru₃**), previously lacking crystallographic characterization, adopts both C_s isomers in solution. In situ ESI-MS studies on the synthesis of **Cs⊂Rh₄Ru₃** revealed two Cs-containing intermediates, **Cs⊂Rh₂Ru₂**⁺ (1239 *m/z*) and **Cs⊂Rh₃Ru₃**⁺ (1791 *m/z*), which underscore the participation of Cs⁺ in the mechanism of cage formation. ¹³³Cs NMR shifts for the cages correlated with the number of CN groups bound to Cs⁺: **Cs⊂Co₄Ru₄**⁺ (δ 1 vs δ 34 for CsOTf), **Cs⊂Rh₄Ru₃** where Cs⁺ is surrounded by ten CN ligands (δ 91), **Cs⊂Co₄Ru₃**, which consists of isomers with 11 and 10 π-bonded CNs (δ 42 and δ 89, respectively). Although {K⊂[Cp*Rh(CN)₃]₄[Cp*Ru]₃} could not be prepared, {NH₄⊂[Cp*Rh(CN)₃]₄[Cp*Ru]₃} (**NH₄⊂Rh₄Ru₃**) forms readily by NH₄⁺-template cage assembly. IR and NMR measurements indicate that NH₄⁺ binding is weak and that the site symmetry is low. CsOTf quantitatively and rapidly converts **NH₄⊂Rh₄Ru₃** into **Cs⊂Rh₄Ru₃**, demonstrating the kinetic advantages of the M₇ cages as ion receptors. Crystallographic characterization of **CsCo₄Ru₃** revealed that it crystallizes in the C_s-(exo)₁(endo)₂ isomer. In addition to the nine μ-CN ligands, two CNₜ ligands are π-bonded to Cs⁺. **M⊂Rh₄Ru₃** (M = NH₄, Cs) crystallizes as the second C_s isomer, that is, (exo)₂(endo)₁, wherein only one CNₜ ligand interacts with the included cation. The distorted framework of **NH₄⊂Rh₄Ru₃** reflects the smaller ionic radius of NH₄⁺. The protons of NH₄⁺ were located crystallographically, allowing precise determination of the novel NH₄···CN interaction. A competition experiment between calix[4]arene-bis(benzocrown-6) and **NH₄⊂Rh₄Ru₃** reveals **NH₄⊂Rh₄Ru₃** has a higher affinity for cesium.

Introduction

Molecular containers are of continuing interest for synthetic chemists due to their realized uses as catalysts,[1,2] sorters,[3] sensors,[4,5] and in cavity directed synthesis.[6,7] Most molecular containers are based on hydrocarbon frameworks.[8] An advantage of inorganic frameworks is their potential rigidity, which should impart size-based selectivity to these supermolecules.[9] It has, however, proven difficult to synthesize inorganic molecular cages that exhibit host–guest behavior. Our approach to inorganic cages entails the use of the rigid organometallic cyanides. Cyanometalate building blocks indeed give rise to diverse structures such as chains,[10,11] triangles,[12,13] squares,[14–16] hexagons,[17] boxes,[18,19] and extended solid frameworks[20] which have been discussed as sensors,[21] molecular magnets,[22,23] and sieves.[24]

Much work on cyanometalate-based cages is inspired by Prussian Blue (PB), the inorganic polymer Fe₇(CN)₁₈(H₂O)ₓ.[25] PB is prepared by the building block approach, the condensation of [Fe(CN)₆]⁴⁻ and Fe(III) salts (eq 1).

$$3[Fe(CN)_6]^{4-} + 4Fe^{3+} \rightarrow Fe_7(CN)_{18}(H_2O)_x \quad (\text{"PB"}) \quad (1)$$
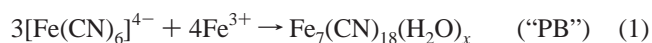
PB consists of CN-interconnected octahedral Fe centers, the

(1) Kang, J.; Santamaria, J.; Hilmersson, G.; Rebek, J., Jr. *J. Am. Chem. Soc.* **1998**, *120*, 7389–7390.
(2) Ito, H.; Kusukawa, T.; Fujita, M. *Chem. Lett.* **2000**, 598–599.
(3) Atwood, J. L.; Koutsantonis, G. A.; Raston, C. L. *Nature* **1994**, *368*, 229–231.
(4) Lehaire, M.-L.; Scopelliti, R.; Piotrowski, H.; Severin, K. *Angew. Chem., Int. Ed.* **2002**, *41*, 1419–1422.
(5) Beer, P. D.; Szemes, F.; Balzani, V.; Sala, C. M.; Drew, M. G. B.; Dent, S. W.; Maestri, M. *J. Am. Chem. Soc.* **1997**, *119*, 11864–11875.
(6) Yoshizawa, M.; Takeyama, Y.; Kusukawa, T.; Fujita, M. *Angew. Chem., Int. Ed.* **2002**, *41*, 1347–1349.
(7) Yoshizawa, M.; Kusukawa, T.; Fujita, M.; Sakamoto, S.; Yamaguchi, K. *J. Am. Chem. Soc.* **2001**, *123*, 10454–10459.
(8) Lehn, J. M. *Supramolecular Chemistry: Concepts and Perspectives*; VCH: Weinheim, 1995.
(9) Huang, S. P.; Kanatzidis, M. G. *Angew. Chem., Int. Ed. Engl.* **1992**, *31*, 787–789.

(10) Chiorboli, C.; Bignozzi, C. A.; Indelli, M. T.; Rampi, M. A.; Scandola, F. *Coord. Chem. Rev.* **1991**, *111*, 267–274.
(11) Scandola, F.; Argazzi, R.; Bignozzi, C. A.; Chiorboli, C.; Indelli, M. T.; Rampi, M. A. *Coord. Chem. Rev.* **1993**, *125*, 283–292.
(12) Evans, W. J.; Drummond, D. K. *Organometallics* **1988**, *7*, 797–802.
(13) Davies, J. A.; Hartley, F. R.; Murray, S. G.; Pierce-Butler, M. A. *J. Chem. Soc., Dalton Trans.* **1983**, 1305–1308.
(14) Martinez, J.; Adams, H.; Bailey, N. A.; Maitlis, P. M. *J. Organomet. Chem.* **1991**, *405*, 393–402.
(15) Schinnerling, P.; Thewalt, U. *J. Organomet. Chem.* **1992**, *431*, 41–45.
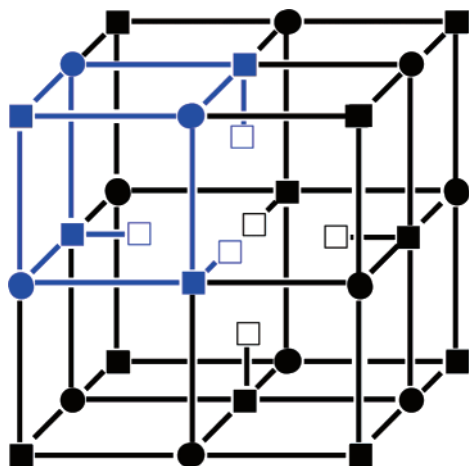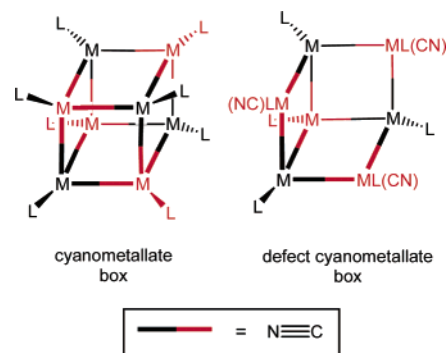(16) Oshio, H.; Yamamoto, M.; Ito, T. *Inorg. Chem.* **2002**, *41*, 5817–5820.

Figure 1. Unit cell for Prussian Blue, $Fe_4[Fe(CN)_6]_3 \cdot 3(H_2O)_6$, as proposed by Ludi et al.[25] ■, Fe(III) (N and O coordination); ●, Fe(II) (C coordination); and □, H_2O. The blue highlighted area represents a defect box subunit.

framework of which defines a series of boxlike subunits (Figure 1). As indicated by its formula, PB consists of many defects, and these defects are integrally related to PB's host−guest behavior.[26,27] Thus, whereas $(LM)_8(CN)_{12}$ cages have been mentioned as molecular representations of PB,[28] lower symmetry derivatives of such cubic cages in fact would be more faithful representations of PB, with regards to both structure and function. Such a defect structure provides context for the present project, which describes a series of heptametallic cyano-bridged cages. PB and some of its analogues exhibit a particular affinity for Cs^+.[29] Improved understanding of cyanometalate−Cs^+ interactions provides a second context for our work, that is, the design of new classes of ion selection agents.[30,31]

In prior work, the 1:1 reaction of $[CpCo(CN)_3]^-$ and $[Cp*Rh-(NCMe)_3]^{2+}$ was shown to afford $\{[CpCo(CN)_3]_4[Cp*Rh]_4\}^{4+}$. This boxlike cage has a van der Waals' void volume of ca. 54 $Å^3$.[19] Subsequently, we found that the related reaction involving $[Cp*Rh(CN)_3]^-$ in place of $[CpCo(CN)_3]^-$ affords the C_{3v} symmetric cage $\{[Cp*Rh(CN)_3]_4[Cp*Rh]_3\}^{2+}$, referred to in this paper as a "defect box" due to its structural similarity to the parent molecular boxes (Scheme 1).[32]

The following lessons were learned from our initial studies on $Cp*Rh^{2+}$-based cages:

(17) Obora, Y.; Ohta, T.; Stern, C. L.; Marks, T. J. *J. Am. Chem. Soc.* **1997**, *119*, 3745−3755.
(18) Heinrich, J. L.; Berseth, P. A.; Long, J. R. *Chem. Commun.* **1998**, 1231−1232.
(19) Klausmeyer, K. K.; Rauchfuss, T. B.; Wilson, S. R. *Angew. Chem., Int. Ed.* **1998**, *37*, 1694−1696.
(20) Beauvais, L. G.; Shores, M. P.; Long, J. R. *Chem. Mater.* **1998**, *10*, 3783−3786.
(21) Beauvais, L. G.; Shores, M. P.; Long, J. R. *J. Am. Chem. Soc.* **2000**, *122*, 2763−2772.
(22) Holmes, S. M.; Girolami, G. S. *J. Am. Chem. Soc.* **1999**, *121*, 5593−5594.
(23) Beauvais, L. G.; Long, J. R. *J. Am. Chem. Soc.* **2002**, *124*, 12096−12097.
(24) Klausmeyer, K. K.; Wilson, S. R.; Rauchfuss, T. B. *J. Am. Chem. Soc.* **1999**, *121*, 2705−2711.
(25) Herren, F.; Fischer, P.; Ludi, A.; Haelg, W. *Inorg. Chem.* **1980**, *19*, 956−959.
(26) Lundgren, C. A.; Murray, R. W. *Inorg. Chem.* **1988**, *27*, 933−939.
(27) Pyrasch, M.; Toutianoush, A.; Jin, W.; Schnepf, J.; Tieke, B. *Chem. Mater.* **2003**, *15*, 245−254.
(28) Sodio, C. N. H.; Ramesh, M.; Espenson, J. H.; Rauchfuss, T. B. *Angew. Chem., Int. Ed.* **2003**.
(29) Dunbar, K. R.; Heintz, R. A. *Prog. Inorg. Chem.* **1997**, *45*, 283−391.
(30) Bryan, J. C.; Kavallieratos, K.; Sachleben, R. A. *Inorg. Chem.* **2000**, *39*, 1568−1572.
(31) Gokel, G. W.; Barbour, L. J.; Ferdani, R.; Hu, J. *Acc. Chem. Res.* **2002**, *35*, 878−886.
(32) Contakes, S. M.; Klausmeyer, K. K.; Milberg, R. M.; Wilson, S. R.; Rauchfuss, T. B. *Organometallics* **1998**, *17*, 3633−3635.

Scheme 1

cyanometallate box   defect cyanometallate box

= N≡C

(1) Cationic cages failed to exhibit detectable host−guest behavior. This finding led to our interest in anionic or charge-neutral cages.

(2) The stoichiometry of the condensing partners significantly influences the course of the condensation.

(3) The steric bulk of the ancillary ligands (e.g., Cp vs Cp*) can be used to modify the box-forming tendencies of these cyanometalates. Because of the relative stereochemistry of the three terminal cyanide ligands (CN_t) in defect cages, their M_7-CN_{12} frameworks are not true subunits of the completed M_8-$(CN)_{12}$ boxes. Addition of $[Cp*Rh(NCMe)_3]^{2+}$ to $\{[Cp*Rh-(CN)_3]_4[Cp*Rh]_3\}^{2+}$ does not lead to cage closure.

(4) The M−CN−M′ linkages are ordered in all known cyanometalate boxes and defect boxes, as shown by ^{13}C NMR and crystallographic studies. Metals with labile M−CN linkages do not form box or defect-box structures.[33,34]

These four points underpin the present study, which originated with our recently reported synthesis of $[CpCo(CN)_3]^-/[Cp*Ru]^+$ cages.[35] These Co−Ru cages, which are less cationic than related $Cp*Rh^{2+}$ derived species, require the presence of a templating cation, Cs^+ being particularly versatile in this regard. We found that the $[CpCo(CN)_3]^-/[Cp*Ru]^+/Cs^+$ reaction affords both $Cs \subset M_7$ defect boxes and $Cs \subset M_8$ boxes, depending on the reaction stoichiometry.[35] We confirmed that $Cs \subset [CpCo(CN)_3]_4$-$[Cp*Ru]_4^+$ (**Cs⊂Co₄Ru₄⁺**)[35] adopts the boxlike structure anticipated by its more labile analogue $\{Cs \subset [Cp*Rh(CN)_3]_4$-$[Mo(CO)_3]_4\}^{3-}$.[24] The structure of the defect box $Cs \subset [CpCo-(CN)_3]_4[Cp*Ru]_3$ (**Cs⊂Co₄Ru₃**), however, is of great interest because it was unclear exactly how the Cs^+ was accommodated by the CN_t (terminal) ligands. NMR studies indicated that **Cs⊂Co₄Ru₃** exists as a mixture of two unsymmetrical isomers, which were proposed to differ in terms of the relative stereochemistry of the Cp and CN_t ligands on the "rim" of the cage (Figure 2). The structure proposed for **Cs⊂Co₄Ru₃** was unprecedented because it involved terminal CN ligands π-bonded to Cs^+. Interest in this cage was enhanced because, despite its existence as isomers, it behaves as a tridentate ligand, somewhat akin to trispyrazolyl borates, triazacyclononane, etc., enabling the formation of novel heterotrimetallic boxes and double boxes (Scheme 2).

The defect boxes represent a novel motif for ion sequestration, as they possess a pocket for guest ions.[28] Whereas the ion exchange rates for the guest in **guest⊂M₄M₄** are quite slow,[28]

(33) Contakes, S. M.; Rauchfuss, T. B. *Angew. Chem., Int. Ed.* **2000**, *39*, 1984−1986.
(34) Contakes, S. M.; Rauchfuss, T. B. *Chem. Commun.* **2001**, 553−554.
(35) Contakes, S. M.; Kuhlman, M. L.; Ramesh, M.; Wilson, S. R.; Rauchfuss, T. B. *Proc. Natl. Acad. Sci. U.S.A.* **2002**, *99*, 4889−4893.
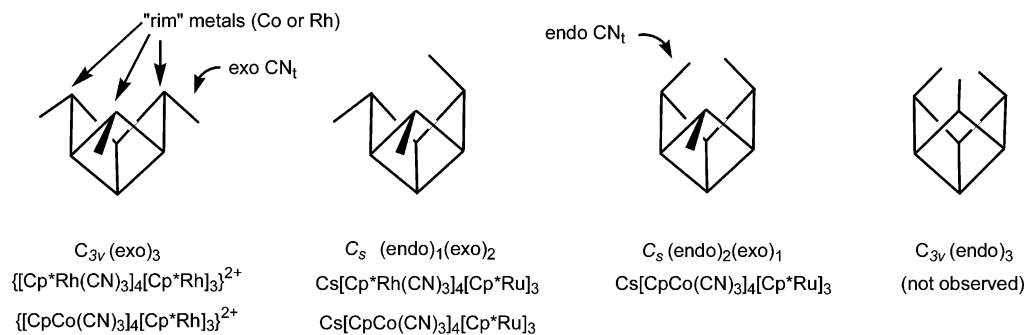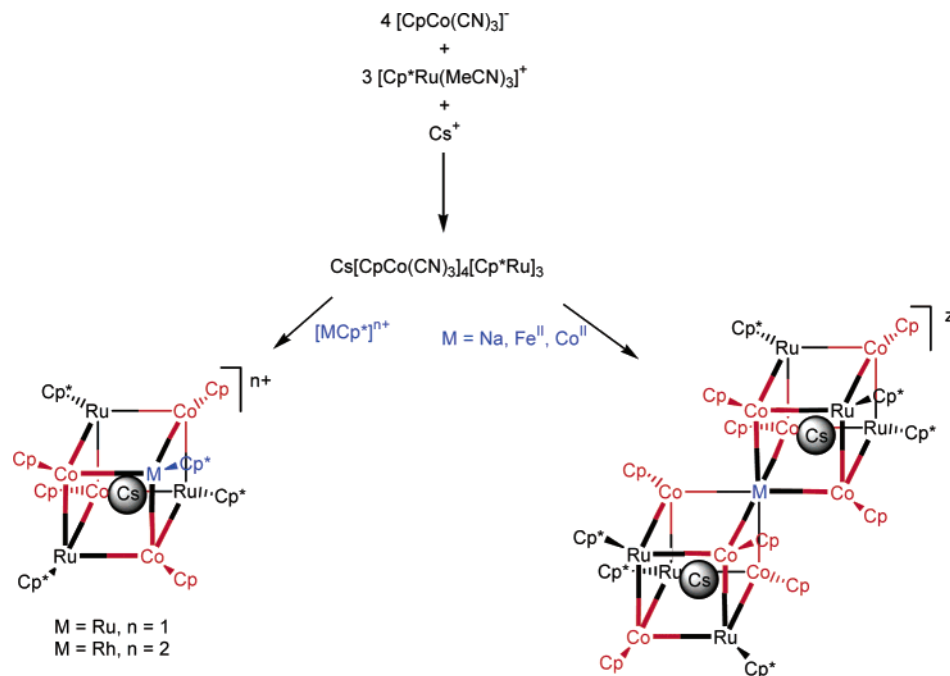
Figure 2. Structural isomers of $(LM)_7(\mu\text{-CN})_9(CN_t)_3$ cages where the lines indicate the CN ligands.
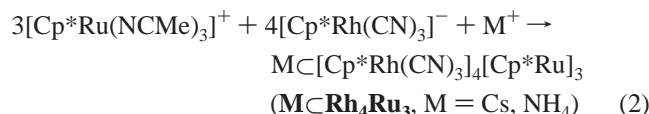
Scheme 2

the ion exchange rates for the defect boxes should be high because of their more open structure. This motif is potentially relevant to the design of new sequestering agents for radiowaste materials.[36,37]

Results and Discussion

I. Synthesis and Reactivity. Synthesis and Characterization of {Cs⊂[Cp*Rh(CN)₃]₄[Cp*Ru]₃}. Reaction of 0.75 equiv of [Cp*Ru(NCMe)₃]PF₆ with Et₄N[Cp*Rh(CN)₃] and 0.25 equiv of CsOTf in MeCN solution produced {Cs⊂[Cp*Rh(CN)₃]₄-[Cp*Ru]₃} (**Cs⊂Rh₄Ru₃**). Golden yellow crystals of the product were obtained in excellent yield (eq 2).

$$3[Cp^*Ru(NCMe)_3]^+ + 4[Cp^*Rh(CN)_3]^- + M^+ \rightarrow$$
$$M \subset [Cp^*Rh(CN)_3]_4[Cp^*Ru]_3$$
$$(\mathbf{M \subset Rh_4Ru_3}, M = Cs, NH_4) \quad (2)$$

The IR spectrum of **Cs⊂Rh₄Ru₃** features ν_{CN} bands at 2158, 2142, 2124, and 2121 cm^{-1}, which are shifted to higher frequencies versus 2124 and 2114 cm^{-1} for free (Et₄N)[Cp*Rh-(CN)₃]. ESI-MS measurements confirmed the formula (m/z =

2107 amu). Signals were not detected for the corresponding box **Cs⊂Rh₄Ru₄**⁺. Purified samples of **Cs⊂Rh₄Ru₃** proved unreactive toward additional [Cp*Ru(NCMe)₃]⁺. Consequently, the stoichiometry of the reaction in eq 2 is not as critical as the synthesis of {Cs⊂[CpCo(CN)₃]₄[Cp*Ru]₃}.[28]

Attempted syntheses of the empty (or voided) anionic bowl {[Cp*Rh(CN)₃]₄[Cp*Ru]₃}⁻ were unsuccessful. Reaction of 0.75 equiv of [Cp*Ru(NCMe)₃]PF₆ with (Et₄N)[Cp*Rh(CN)₃] resulted in insoluble solids. Such negative results, which are reminiscent of the untemplated reactions of [Cp*Ru(NCMe)₃]⁺ and [CpCo(CN)₃]⁻,[35] underscore the important role of the Cs⁺ template.

ESI-MS Studies on Cage Assembly. In contrast to **Cs⊂Co₄-Ru₃**, the all-Cp* cage **Cs⊂Rh₄Ru₃** exhibits good solubility in MeCN despite the fact that it is charge-neutral. This property enabled us to monitor the cage-forming process by ESI-MS measurements on homogeneous MeCN solutions. Analysis of the crude reaction mixture by ESI-MS was hindered by the presence of Et₄NPF₆, which dominates the ion current. ESI-MS analysis of reaction mixtures revealed no anionic cage intermediates in the cage formation process − only PF₆⁻ was

(36) Sachleben, R. A.; Urvoas, A.; Bryan, J. C.; Haverlock, T. J.; Moyer, B. A.; Hay, B. P. *Chem. Commun.* **1999**, 1751−1752.

(37) Casnati, A.; Pochini, A.; Ungaro, R.; Ugozzoli, F.; Arnaud, F.; Fanni, S.; Schwing, M.-J.; Egberink, R. J. M.; de Jong, F.; Reinhoudt, D. N. *J. Am. Chem. Soc.* **1995**, *117*, 2767−2777.
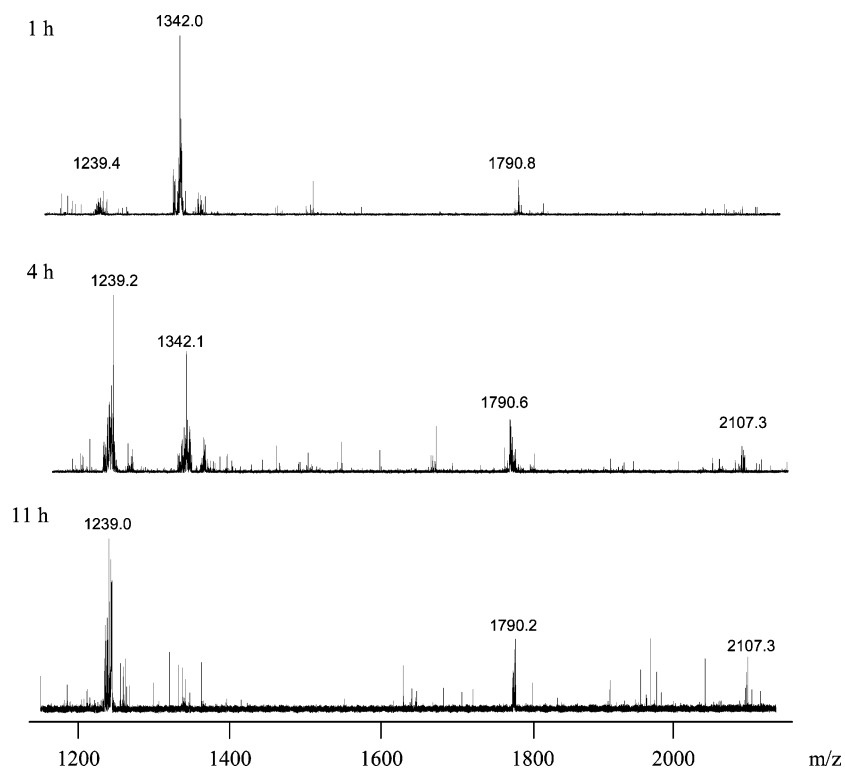
Figure 3. ESI-MS spectra at 1, 4, and 11 h for the reaction of 0.25 equiv of Cs$^+$, Cp*Rh(CN)$_3$$^-$, and 0.75 equiv of Cp*Ru(MeCN)$_3$$^+$ leading ultimately to the formation of **Cs⊂Rh$_4$Ru$_3$**. Assignments: **Cs⊂Rh$_2$Ru$_2$$^+$** (1239 *m/z*), **Rh$_2Ru_3$$^+$** (1342 *m/z*), **Cs⊂Rh$_3Ru_3$$^+$** (1791 *m/z*), as well as the product, **Cs⊂Rh$_4$Ru$_3$** (2107 *m/z*).

observed. Under normal synthesis conditions, the formation of **Cs⊂Rh$_4$Ru$_3$** requires 24 h, and, during this time, three intermediates were observed, **Cs⊂Rh$_2$Ru$_2$$^+$** (1239 amu), **Rh$_2Ru_3$$^+$** (1342 amu), **Cs⊂Rh$_3Ru_3$$^+$** (1791 amu), as well as the product [**Cs⊂Rh$_4$Ru$_3$**] (2107 amu). The first product to appear is **Rh$_2$Ru$_3$$^+$** (Figure 3). Over the course of hours, this intermediate is consumed concomitant with the appearance of both **Cs⊂Rh$_2$-Ru$_2$$^+$** and **Cs⊂Rh$_3Ru_3$$^+$**, as well as the final product. Monitoring the reaction revealed that the amount of final product increased concomitant with the decrease in the proposed intermediates, suggesting they are true intermediates and not a side product of the reaction. MS/MS measurements showed that these cations do not arise from fragmentation of **Cs⊂Rh$_4$Ru$_3$**. ESI-MS analysis revealed that "NMR-pure" samples of **Cs⊂Rh$_4$Ru$_3$** contain trace impurities of **Cs⊂Rh$_2$Ru$_2$$^+$** and **Cs⊂Rh$_3Ru_3$$^+$**, which can be removed by further recrystallization. This fact indicates that these smaller cages may in fact be isolable, although this was not explored.

The admittedly limited ESI-MS data can be rationalized in the context of a tentative mechanism for the formation of **Cs⊂Rh$_4$Ru$_3$**. An initially formed charge-neutral square **Rh$_2$Ru$_2$**, which would not be easily detected by ESI-MS, would bear terminal CN ligands attractive toward Cp*Ru$^+$ centers. The resulting **Rh$_2$Ru$_3$$^+$** apparently undergoes an exchange process of Cp*Ru$^+$ for Cs$^+$ leading to **Cs⊂Rh$_2$Ru$_2$$^+$**. Thereafter, the cage growth process is proposed to follow an alternating addition of anionic [Cp*Rh(CN)$_3$]$^-$ and cationic Cp*Ru$^+$ centers. One clear conclusion from these measurements is that Cs$^+$ participates in the early stages of cage assembly.

^{133}Cs NMR Measurements. ^{133}Cs NMR spectroscopy provided a useful tool for characterizing these Cs-containing cage compounds. Not only do the spectra allow one to assay the

purity of cage samples, the chemical shift was found to correlate with the number of η^2-CN ligands surrounding the Cs$^+$ ion (Figure 4). **Cs⊂Co$_4$Ru$_4$$^+$** with all 12 cyanides interacting with Cs$^+$ resulted in a signal at δ 1 versus δ 34 for CsOTf, which we attribute to maximal shielding relative to the other cases. In **Cs⊂Rh$_4$Ru$_3$**, where Cs$^+$ is surrounded by only 10 CN ligands, the ^{133}Cs signal occurs at δ 91. Key interpolations come from measurements on **Cs⊂Co$_4$Ru$_3$**, which consists of two isomers, one of which has 11 CN ligands interacting with Cs$^+$ and the other with 10 (vide infra). The dominant signal at δ 42 is assigned as the isomer with a Cs(CN)$_{11}$ site, that is, the isomer that crystallizes (allowing us to assign the ^{1}H NMR signals to particular isomers). The minor signal (δ 89) is assigned to the isomer with a Cs(CN)$_{10}$ site, as for **Cs⊂Rh$_4$Ru$_3$**. The ^{133}Cs MAS NMR spectrum for a solid sample of **Cs⊂Rh$_4$Ru$_3$** was inconclusive, showing one broad peak within the range of both isomers (δ 63).

{NH$_4$⊂[Cp*Rh(CN)$_3$]$_4$[Cp*Ru]$_3$}. The fact that the voided cage [**Rh$_4$Ru$_3$**]$^-$ could not be synthesized indicates that complexation to cations is important for cage stability, as well as cage formation (see above). On the basis of our inability to synthesize **K⊂Rh$_4$Ru$_3$**, we concluded that K$^+$ (r_{ionic} = 1.52 Å) is too small. In contrast, NH$_4$$^+$ (r_{ionic} = 1.75 Å), which is only 0.06 Å smaller than Cs$^+$, does template the formation of a defect box. The addition of 0.75 equiv of [Cp*Ru(NCMe)$_3$]$^+$ to a MeCN solution of Et$_4$N[Cp*Rh(CN)$_3$] in the presence of 0.25 equiv of NH$_4$PF$_6$ efficiently produced NH$_4$⊂[CpCo(CN)$_3$]$_4$-[Cp*Ru]$_3$ (**NH$_4$⊂Rh$_4$Ru$_3$**, eq 2). ESI-MS measurements confirmed the formula, with M$^+$ at *m/z* = 1992 amu. With regards to the less hindered cages, we have been unable to synthesize **M⊂Co$_4$Ru$_3$** for any M other than Cs.

The IR spectrum of **NH$_4$⊂Rh$_4$Ru$_3$** in the ν_{NH} region indicated
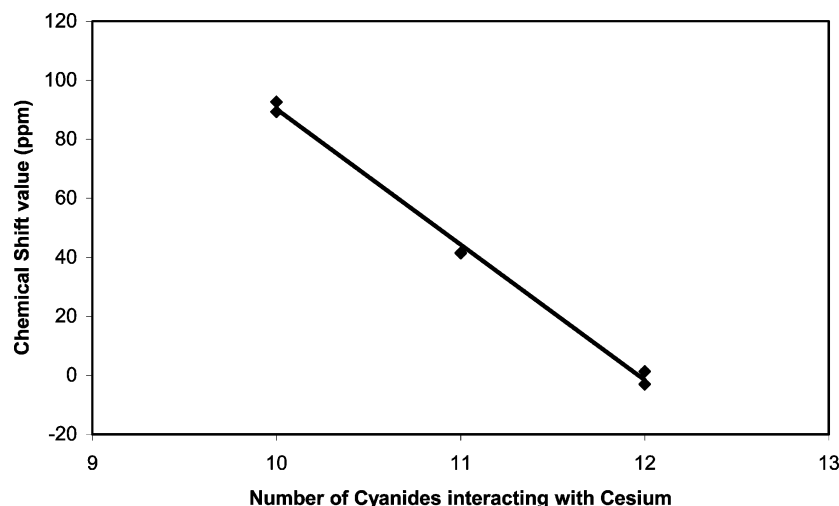
Figure 4. Plot of ^{133}Cs NMR chemical shift vs number of π-CN^- ligands interacting with the Cs^+. Data: **Cs⊂Co₄Ru₄⁺** (δ 1), two isomers of **Cs⊂Co₄Ru₃** (δ 89 for minor isomer, 42 for major isomer), **Cs⊂Rh₄Ru₃** (δ 91), and Cs⊂{[Cp*Rh(CN)₃]₄[Mo(CO)₃]₄}³⁻ (−δ 3).
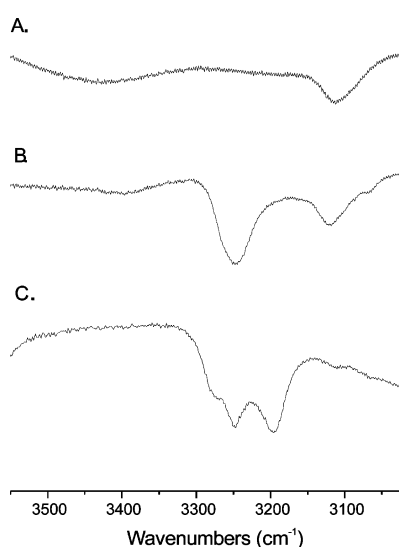
Figure 5. IR spectra (KBr pellets) in the ν_{NH} region for **Co₄Ru₄** (A) as a blank, **NH₄⊂Co₄Ru₄⁺** (B),[28] and **NH₄⊂Rh₄Ru₃** (C).

that the cation is bound in an unsymmetrical environment. Peaks were observed at 3196, 3246, and 3270 (sh) cm^{-1}. In contrast, the IR spectrum of **NH₄⊂Co₄Ru₄⁺** shows only one peak at 3250 cm^{-1} assigned to the T_2 mode reflecting a symmetrical environment (Figure 5). In **NH₄⊂Rh₄Ru₃**, the T_2 mode has split into E and A_1 modes, while the A_1, previously only Raman-active, becomes IR-active due to the decreased site symmetry.[38] This low site symmetry arises not only from the overall cage structure, but more specifically from the unique N−H···NC interaction between the endo CN_t and one of four NH bonds (vide infra). Typical strong X···HNH_3^+ hydrogen bonds exhibit two energetically distinct ν_{N-H} bands. Isolated N−H units exhibit $\nu_{N-H} \approx 3400-3260$ cm^{-1}, whereas for N−H···X-containing species $\nu_{N-H} \approx 2975-3110$ cm^{-1}.[39] For **NH₄⊂Rh₄-Ru₃**, $\Delta\nu_{NH} = 50$ cm^{-1}, which indicates a weak interaction between NH_4^+ and the π-bond of CN_t. The T_2 bending mode of NH_4^+ is obscured by the ν_{C-H} bands for the facially capping Cp and Cp* ligands at 1600−1200 cm^{-1}.

(38) Zecchina, A.; Marchese, L.; Bordiga, S.; Paze, C.; Gianotti, E. *J. Phys. Chem. B* **1997**, *101*, 10128−10135.
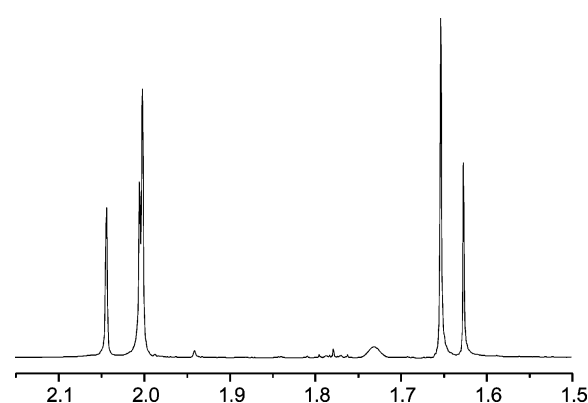(39) Sauer, J.; Ugliengo, P.; Garrone, E.; Saunders, V. R. *Chem. Rev.* **1994**, *94*, 2095−2160.

Figure 6. 500 MHz ^1H NMR spectrum of **NH₄⊂Rh₄Ru₃** (THF solution). The 1:1:2 Cp*Rh and 2:1 Cp*Ru patterns are consistent with one C_s isomer.
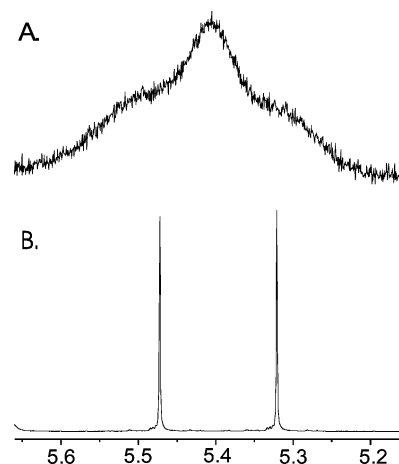
Figure 7. 500 MHz ^1H NMR spectrum of the NH_4^+ region for unenriched **NH₄⊂Rh₄Ru₃** (A) and **¹⁵NH₄⊂Rh₄Ru₃** (B) in THF solutions.

As for **Cs⊂Rh₄Ru₃**, **NH₄⊂Rh₄Ru₃** exists as one isomer in MeCN solution as shown by ^1H NMR spectroscopy (Figure 6). A broad multiplet is observed at δ 5.40 for the NH_4^+ signal. The ^1H NMR spectrum of **¹⁵NH₄⊂Rh₄Ru₃** exhibits a doublet at δ 5.40, demonstrating that the cation is tumbling fast on the NMR time scale inside of the cage (Figure 7). In MeCN solutions, **NH₄⊂Rh₄Ru₃** undergoes rapid exchange H−D exchange with D_2O, demonstrating that the ammonium ion is
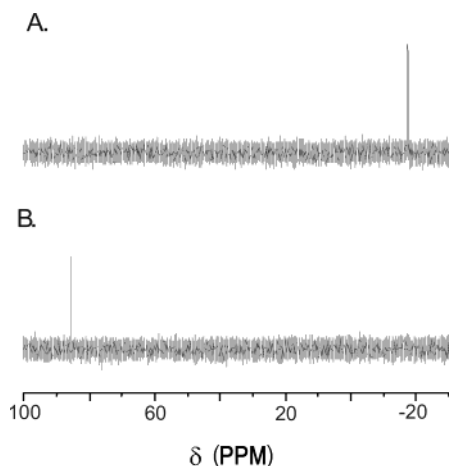
Figure 8. 76 MHz ^{133}Cs NMR spectrum of [Cs(BCB6)]$^+$ (in MeCN solution) before (A) and after (B) treatment with 1 equiv of **NH$_4$⊂Rh$_4$Ru$_3$**. The δ 88 signal corresponds to **Cs⊂Rh$_4$Ru$_3$**.

highly accessible to the solution. Similar experiments show that **NH$_4$⊂Co$_4$Ru$_4$**$^+$ is unreactive toward H−D exchange under these conditions, reflecting the chemical shielding afforded by the completed box.[28] Addition of CsOTf to a MeCN solution of **NH$_4$⊂Rh$_4$Ru$_3$** quantitatively affords **Cs⊂Rh$_4$Ru$_3$** within 20 min.

Affinity of NH$_4$⊂Rh$_4$Ru$_3$ for Cs$^+$. The affinity of **NH$_4$⊂Rh$_4$-Ru$_3$** for Cs$^+$ was qualitatively examined in a competition experiment using calix[4]arene-bis(benzocrown-6) (**BC6B**, Figure 8), a representative member for high-affinity ($K_{eq} = 10^6$) cesium-selective calix[4]arene-crown-6 ligands.[40−44] A MeCN solution of [Cs(BC6B)]$^+$ (^{133}Cs NMR: −δ 17) was treated with 1 equiv of **NH$_4$⊂Rh$_4$Ru$_3$**, resulting within the time required for NMR analysis in quantitative conversion to **Cs⊂Rh$_4$Ru$_3$** (δ 88, see eq 3, Figure 8). The Cs$^+$/K$^+$ and Cs$^+$/Na$^+$ selectivities have not been determined, but our inability to synthesize **K⊂Rh$_4$Ru$_3$** suggests these selectivity values are quite high.
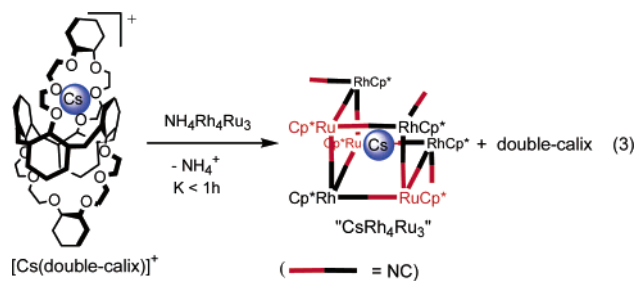
II. Structural Analyses. Isomerism in the Defect Boxes. Defect boxes could, in principle, adopt four isomeric structures, depending on the relative orientation of the three CN$_t$ ligands (see Figure 2). ^{1}H NMR measurements show that **Cs⊂Rh$_4$Ru$_3$** exists as one of the two C_s isomers, as demonstrated by the observation of five Cp* signals in a ratio 1:1:2:2:1. In contrast,

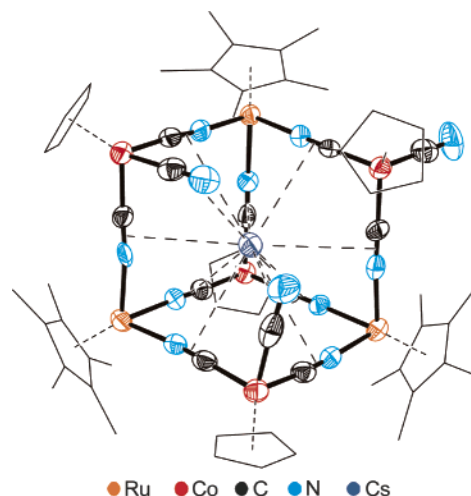(40) Haverlock, T. J.; Mirzadeh, S.; Moyer, B. A. *J. Am. Chem. Soc.* **2003**, *125*, 1126−1127.
(41) Casnati, A.; Sansone, F.; Dozol, J.-F.; Rouquette, H.; Arnaud-Neu, F.; Byrne, D.; Fuangswasdi, S.; Schwing-Weill, M.-J.; Ungaro, R. *J. Inclusion Phenom. Macrocyclic Chem.* **2001**, *41*, 193−200.
(42) Lamare, V.; Dozol, J.-F.; Fuangswasdi, S.; Arnaud-Neu, F.; Thuéry, P.; Nierlich, M.; Asfari, Z.; Vicens, J. *J. Chem. Soc., Perkin Trans. 2* **1999**, 271−284.
(43) Lamare, V.; Dozol, J.-F.; Ugozzoli, F.; Casnati, A.; Ungaro, R. *Eur. J. Org. Chem.* **1998**, 1559−1568.
(44) Thuéry, P.; Nierlich, M.; Bryan, J. C.; Lamare, V.; Dozol, J.-F.; Asfari, Z.; Vicens, J. *J. Chem. Soc., Dalton Trans.* **1997**, 4191−4202.

Figure 9. Molecular structure of **Cs⊂[CpCo(CN)$_3$]$_4$[Cp*Ru]$_3$** showing the atom labeling scheme. Thermal ellipsoids are drawn at the 50% level.

Scheme 3
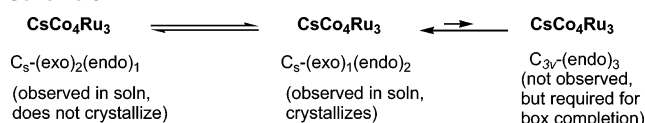
^{1}H NMR spectra for solutions of **CsCo$_4$Ru$_3$** reveal the presence of two unsymmetrical (C_s) isomers, each of which show characteristic subspectra, which can now be assigned on the basis of the ^{133}Cs NMR data (see above). ^{1}H NMR experiments (−60 to 60 °C) did not reveal any line-broadening. If coalescence temperature is conservatively estimated to be 20 °C above 60 °C, this would imply that the rate constant for exo−endo isomerization would have an upper limit of 50 s$^{−1}$. In solution, the cage **CsCo$_4$Ru$_3$** is rapidly capped (box-completion reaction) with various electrophiles,[35] such as Na$^+$ and Cp*Rh^{2+}, and this process is complete within minutes at room temperature (the time required to prepare sample for NMR analysis). Assuming that the rate of complexation is determined by the unimolecular rate of exo−endo isomerization, the speed of the box completion reaction indicates that the speed of the exo−endo isomerization is 0.05 s$^{−1}$.

The ^{1}H NMR spectrum of a solution freshly prepared from single crystals of **Cs⊂Co$_4$Ru$_3$** revealed the presence of the same two C_s isomers in the equilibrium ratio. The rapid isomerization of the cage is related to the ease with which it undergoes box-completion reactions.[35]

The dynamic structure of **Cs⊂Co$_4$Ru$_3$** is evident from the fact that we only isolate one isomer when we can observe two in solution. Furthermore, the facility with which this cage undergoes box-completion reactions implies that all three CN$_t$ ligands can transiently, at least, adopt the all-endo geometry, thereby presenting incoming electrophiles with a tridentate ligand. These assumptions and facts can be accommodated by a mechanism of isomerization that involves the $C_s−C_{3v}−C_s$ process shown in the Scheme 3. An alternative mechanism is that the electrophile caps the C_s-(exo)$_1$(endo)$_2$ isomer and then isomerization occurs resulting in the C_{3v} product.

Crystallographic Analysis of {Cs⊂[CpCo(CN)$_3$]$_4$[Cp*Ru]$_3$}. Crystallographic characterization of **Cs⊂Co$_4$Ru$_3$** showed that it crystallizes as the C_s-(exo)$_1$(endo)$_2$ isomer (Figure 9, Table 1). Thus, although the ^{1}H and ^{133}Cs NMR data (see above)

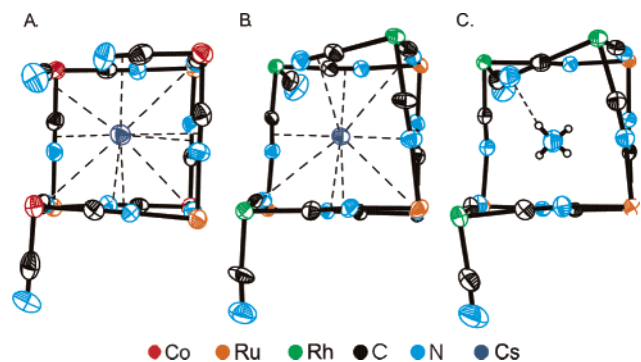**Figure 10.** The view is approximately parallel to two of the Co₂Rh₂(CN)₄ faces so as to show the outward or inward bending of the terminal M(CN)₃ units (M = Co, Rh). (A) **Cs⊂Co₄Ru₃**, (B) **Cs⊂Rh₄Ru₃**, (C) **NH₄⊂Rh₄Ru₃**.

Table 1. Selected Bond Distances (Å) for the Cations in **Cs⊂Co₄Ru₃** and **Cs⊂Rh₄Ru₃**

parameter	Cs⊂Co₄Ru₃	Cs⊂Rh₄Ru₃
C(1)−Cs(1)	3.651(8)	3.512(14)
C(2)−Cs(1)	3.704(8)	3.451(14)
C(3)−Cs(1)	3.661(8)	3.540(15)
C(4)−Cs(1)	3.647(8)	exo-CNₜ
C(5)−Cs(1)	3.767(8)	3.821(16)
C(6)−Cs(1)	3.729(8)	3.748(16)
C(7)−Cs(1)	exo-CNₜ	3.644(14)
C(8)−Cs(1)	3.517(7)	3.919(16)
C(9)−Cs(1)	3.567(8)	exo-CNₜ
C(10)−Cs(1)	3.864(8)	3.700(15)
C(11)−Cs(1)	3.551(8)	3.641(14)
C(12)−Cs(1)	3.606(9)	3.402(15)
N(1)−Cs(1)	3.526(6)	3.525(12)
N(2)−Cs(1)	3.677(6)	3.357(12)
N(3)−Cs(1)	3.587(6)	3.580(12)
N(4)−Cs(1)	3.518(6)	exo-CNₜ
N(5)−Cs(1)	3.665(7)	3.532(12)
N(6)−Cs(1)	3.649(8)	3.603(13)
N(7)−Cs(1)	exo-CNₜ	3.344(12)
N(8)−Cs(1)	3.552(6)	3.795(13)
N(9)−Cs(1)	3.598(6)	exo-CNₜ
N(10)−Cs(1)	3.871(9)	3.715(13)
N(11)−Cs(1)	3.470(6)	3.579(12)
N(12)−Cs(1)	3.433(9)	3.250(13)

indicated the presence of both C_s isomers in solution, only one isomer crystallizes. Three types of Cp*Co(CN)₃ centers are observed in a 1:1:2 ratio as well as two types of Cp*Ru centers. Nine of the twelve CN ligands form Co−CN−Ru bridges; the remaining three CN groups are terminal with two endo and one exo. The endo CNₜ groups interact with Cs⁺, with average Nₜ···Cs and Cₜ···Cs distances of 3.56 and 3.67 Å, respectively. The nine μ-CN ligands are slightly less strongly bound to Cs⁺ with Cs···N distances (3.61 Å) again being shorter than the C···Cs distances (3.66 Å),[45] although it appears that the CNₜ is slightly more strongly bound to Cs than is μ-CN. Typical Cs···NC distances range from 3.113 to 3.678 Å[46,47] with an average distance of 3.28 ± 0.16 Å.[48] With respect to distortions of the overall M₇(CN)₁₂ framework, the Co₂Ru₂(CN)₄ face bearing the exo-CN is slightly bowed inward (Figure 10). The extent of this distortion is indicated by the Co···Co distances within the

(45) Williams, J. M.; Johnson, P. L.; Schultz, A. J.; Coffey, C. C. *Inorg. Chem.* **1978**, *17*, 834−839.

(46) Werner, B.; Kraeuter, T.; Neumueller, B. *Organometallics* **1996**, *15*, 3746−3751.

(47) Ponomareva, V. V.; Skopenko, V. V.; Domasevitch, K. V.; Sieler, J.; Gelbrich, T. *Z. Naturforsch., B: Chem. Sci.* **1997**, *52*, 901−905.

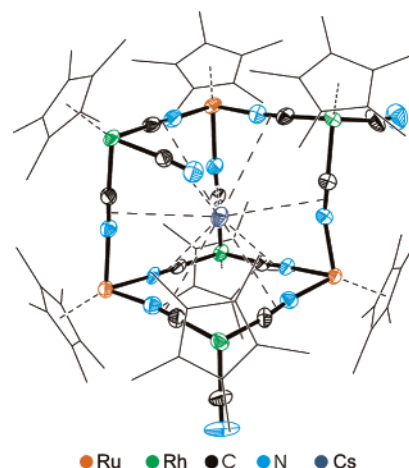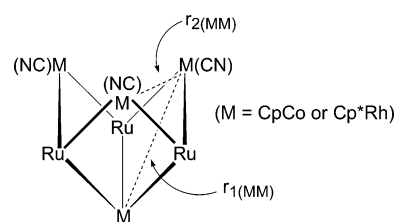(48) Cambridge Structural Database version 5.24, search of Cs−NC distances (16 examples).

Figure 11. Molecular structure of **Cs⊂[Cp*Rh(CN)₃]₄[Cp*Ru]₃** showing the atom labeling scheme. Thermal ellipsoids are drawn at the 50% level.

Scheme 4

Co₂Rh₂(CN)₄ rings, defined as r_{1CoCo}, versus the Co···Co distances between the CpCo(CNₜ) centers, defined as r_{2CoCo} (Scheme 4). Of the three r_{2CoCo} values, two are ∼0.16 Å (2.2%) shorter and one is 0.23 Å (3.2%) longer versus $(r_{1CoCo})_{avg}$.

Crystallographic Analysis of {Cs⊂[Cp*Rh(CN)₃]₄[Cp*-Ru]₃}. **Cs⊂Rh₄Ru₃** adopts the second C_s-(exo)₂(endo)₁ isomer − the one that did not crystallize for **Cs⊂Co₄Ru₃** (Figure 11, Table 1). For the endo CNₜ, the N···Cs distance of 3.25 Å is ca. 0.11 Å shorter than the other nine N···Cs distances, which average 3.59 Å.[49] Similarly, the C···Cs distance of 3.40 Å is shorter than the other Cs···C distances, which average 3.67 Å. The bending of the Rh−C−N linkages in **Cs⊂Rh₄Ru₃** arises from the Cs···N distances again being ca. 0.10 Å shorter than the average Cs···C distance. The Cs atom is unsymmetrically situated with respect to the three Rh atoms at the rim of the defect box: Cs···Rh$_{rim}$(CNₜ)$_{exo}$ = 4.77 Å versus Cs···Rh$_{rim}$(CNₜ)$_{endo}$ = 4.41 Å, while the "nonrim" Rh has a Cs···Rh = 4.31 Å.

The metal cyanide framework of **Cs⊂Rh₄Ru₃** is more distorted than that in **Cs⊂Co₄Ru₃** resulting from two Rh₂Ru₂-(CN)₄ faces being bowed outward, whereas the third face is significantly bowed inward (Figure 10). Using the metrical definitions described above, two r_{2RhRh} are 0.39 Å (5.2%) shorter and the one is 0.47 Å (6.3%) longer versus $(r_{1RhRh})_{avg}$.

Crystallographic Analysis of {NH₄⊂[Cp*Rh(CN)₃]₄[Cp*-Ru]₃}. Of three cages described in this paper, **NH₄⊂Rh₄Ru₃** is the most distorted, reflecting the smaller ionic radius of NH₄⁺ (Figure 12). The unique CNₜ is tilted toward the included cation, more so than in **Cs⊂Rh₄Ru₃** (Figure 13). This added tilting of the unique cyanide bows this **Rh₂Ru₂** face further inward, causing the other two faces to bow out further (Figure 10). From the above terminology, two r_{2RhRh} are 0.59 Å (7.9%) shorter,

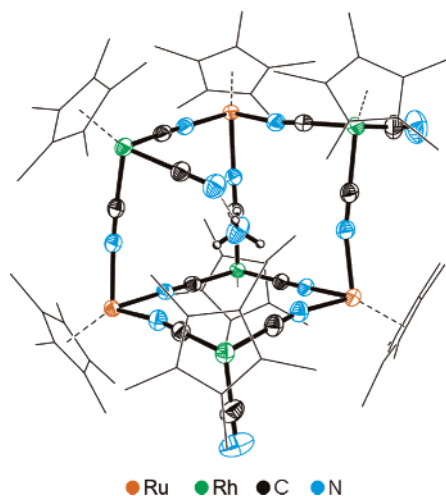(49) Johnson, P. L.; Koch, T. R.; Williams, J. M. *Acta Crystallogr., Sect. B* **1977**, *B33*, 1293−1295.

● Ru   ● Rh   ● C   ● N

Figure 12. Molecular structure of **NH₄⊂[Cp*Rh(CN)₃]₄[Cp*Ru]₃** showing the atom labeling scheme. Thermal ellipsoids are drawn at the 50% level.
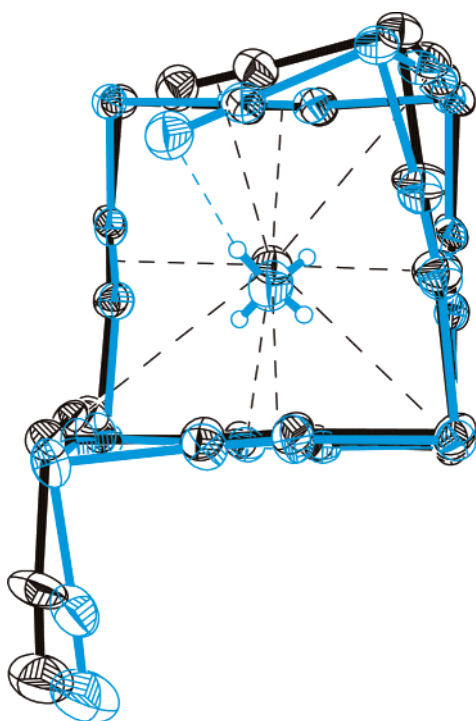
Figure 13. Overlay of **NH₄⊂Rh₄Ru₃** (blue) and **Cs⊂Rh₄Ru₃** (black).

while the unique r_{2RhRh} is 0.46 Å (6.1%) longer than $(r_{1RhRh})_{avg}$. The distortion is also evident in the comparison of Rh···N distances. The NH₄⁺ is unsymmetrically situated with respect to the four Rh atoms: N···Rh$_{rim}$(CN$_t$)$_{exo}$ = 4.78 Å versus N···Rh$_{rim}$(CN$_t$)$_{endo}$ = 4.38 Å, while the "nonrim" Rh has a N···Rh = 4.14 Å. Thus, the cation in **NH₄⊂Rh₄Ru₃** is more deeply embedded into the M₇(μ-CN)₉ cavity (Figure 13).

The four protons of NH₄⁺ were located with an average N—H distance of 0.80 Å. The H₄N···N$_t$C distance is 2.95 Å, and the H₃N—H···N$_t$C distance is 2.14 Å (Figure 12), which is typical of H₃N—H···N hydrogen bonds.[50-53] In contrast to **Cs⊂Rh₄Ru₃**,

(50) Wallwork, S. C. *Acta Crystallogr.* **1962**, *15*, 758−759.
(51) Graf, E.; Kintzinger, J. P.; Lehn, J. M.; LeMoigne, J. *J. Am. Chem. Soc.* **1982**, *104*, 1672−1678.
(52) Johnson, P. L.; Schultz, A. J.; Underhill, A. E.; Watkins, D. M.; Wood, D. J.; Williams, J. M. *Inorg. Chem.* **1978**, *17*, 839−844.

all three of the M₄(CN)₄ faces in [Cp*Rh(CN)₃]₄[Cp*Rh]₃(PF₆)₂ are significantly bowed outward, apparently due to repulsions between Cp*Rh(CN$_t$) centers. The Ru₂Rh₂(CN$_t$)$_{endo}$ face of **Cs⊂Rh₄Ru₃** is bowed inward toward Cs⁺, arising from a short Cs···N distance of 3.25 (vs van der Waals radii for Cs···N, ~3.3).

Summary

In this work, the structural chemistry of cation-containing defect cyanometalate boxes was elucidated. The less bulky derivative **Cs⊂Co₄Ru₃** is an interesting building block for new boxlike and double box cage structures.[35] The defect box also represents a promising motif for cation receptors because, unlike the corresponding completed boxes,[28] these cations are more solvent-accessible and hence more kinetically labile.

Specific conclusions follow:

(1) Whereas the first example of a defect box, [Cp*Rh(CN)₃]₄-[Cp*Rh]₃²⁺, featured all exo-CN$_t$ ligands,[32] the cation-containing defect boxes have one or two endo-CN$_t$ ligands. These endo-CN$_t$ ligands interact ionically with the guest cation.

(2) The steric profile of the coligands (Cp* vs Cp) allows one to enforce the defect box motif without box formation. Whereas **Cs⊂Co₄Ru₃** is reactive toward metal electrophiles to give boxlike cages, the all-Cp* species **Cs⊂Rh₄Ru₃** show no affinity for "capping" metal electrophiles.

(3) ¹³³Cs NMR spectroscopy provides a convenient indicator of the Cs⁺ coordination environment in cyanometalates.

(4) The successful synthesis of **NH₄⊂Rh₄Ru₃** defines the dimensions critical for cage formation: NH₄⁺ (r_{ionic} = 1.75 Å) being intermediate in size between K⁺ (r_{ionic} = 1.52 Å), which does not react, and Cs⁺ (r_{ionic} = 1.81 Å). **NH₄⊂Rh₄Ru₃** binds Cs⁺ tightly and, in contrast to **NH₄⊂Co₄Ru₄⁺**,[28] ion-exchanges rapidly.

(5) Structural analyses of the two defect boxes, **Cs⊂Co₄Ru₃**, **NH₄⊂Rh₄Ru₃**, and **Cs⊂Rh₄Ru₃**, reveal that cage distortion increases as the cationic guest becomes smaller or the Cp groups become larger.

(6) A competition experiment between a well-known cesium selective complexant demonstrates that **NH₄⊂Rh₄Ru₃** has a high affinity for cesium.

Materials and Methods

General. Standard Schlenk techniques were employed in all syntheses. Et₄N[Cp*Rh(CN)₃],[19] [Cp*Ru(NCMe)₃]PF₆,[54] {Cs⊂[CpCo-(CN)₃]₄[Cp*Ru]₃},[35] CsOTf, and NH₄PF₆ were either prepared according to literature methods or purchased from Aldrich. Because the purity of [Cp*Ru(NCMe)₃]PF₆ proved critical, the as-synthesized salt was further recrystallized from CH₂Cl₂−Et₂O to give a bright yellow microcrystalline solid. Elemental analyses were conducted by the School of Chemical Sciences Microanalytical Laboratory. ¹³C and ¹H NMR spectra were acquired on Varian Unity 400 and 500 NMR spectrometers. Infrared spectra were acquired on a Mattson Infinity Gold FTIR spectrometer using CaF₂ solution cells or with KBr pellets. Electrospray ionization-mass spectra (ESI-MS) and MS/MS measurements were acquired using a Micromass Quattro QHQ quadrupole−hexapole−quadrupole instrument.

Cs⊂[Cp*Rh(CN)₃]₄[Cp*Ru]₃ (Cs⊂Rh₄Ru₃). A solution of 384 mg (0.762 mmol) of purified [Cp*Ru(NCMe)₃]PF₆ in 20 mL of MeCN was added dropwise to a solution of 72 mg (0.254 mmol) of CsOTf and 457 mg (1.017 mmol) of Et₄N[Cp*Rh(CN)₃] in 25 mL of MeCN.

(53) Virovets, A. V.; Fedin, V. P.; Samsonenko, D. G.; Clegg, W. *Acta Crystallogr., Sect. C: Cryst. Struct. Commun.* **2000**, *C56*, 272−273.
(54) Fagan, P. J.; Ward, M. D.; Calabrese, J. C. *J. Am. Chem. Soc.* **1989**, *111*, 1698−1719.

Table 2. Crystallographic Data for **Cs⊂Co₄Ru₃**, **Cs⊂Rh₄Ru₃**, and **NH₄⊂Rh₄Ru₃**

	Cs⊂Co₄Ru₃	Cs⊂Rh₄Ru₃	NH₄⊂Rh₄Ru₃
chemical formula	$C_{62}H_{65}Co_4CsN_{12}Ru_3$	$C_{82}H_{105}CsN_{12}Rh_4Ru_3$	$C_{82}H_{109}N_{13}Rh_4Ru_3$
temp (K)	193(2)	193(2)	193(2)
crystal size (mm³)	0.24 × 0.16 × 0.10	0.60 × 0.40 × 0.40	0.65 × 0.20 × 0.18
space group	$P2(1)/c$	$P2_1/n$	$Pnma$
a (Å)	15.414(7)	14.926(12)	25.987(10)
b (Å)	25.048(12)	48.475(4)	17.203(6) A
c (Å)	23.332(11)	16.093(12)	23.432(9) A
α (deg)	90	90	90
β (deg)	104.807(10)	104.076(5)	90
γ (deg)	90	90	90
V (Å³)	8709(7)	11 293.9(15)	10 475(7)
Z	4	4	4
D_{calcd} (Mg m⁻³)	1.540	1.480	1.403
μ (Mo Kα, mm⁻¹)	1.715	1.330	1.084
min and max trans'n	0.6066/0.8481	0.4688/0.6957	0.5294/0.8395
reflections meas'd/indep.	45 846/15 947	67 845/19 946	103 582/9981
data/restraints/parameters	15 947/27/955	19 946/994/991	9981/161/675
GOF	0.876	1.341	1.050
R_{int}	0.0680	0.0419	0.0485
R_1 [$I > 2\sigma$] (all data)[a]	0.0651 (0.1399)	0.1215 (0.1285)	0.0284 (0.0355)
wR_2 [$I > 2\sigma$] (all data)[b]	0.1555 (0.1882)	0.2541 (0.2569)	0.0672 (0.0698)
max peak/hole (e/Å³)	2.806/−1.155	3.225/−2.090	0.589/−1.565

[a] $R_1 = \sum||F_o| - |F_c||/\sum|F_o|$. [b] $wR_2 = \{\sum[w(F_o^2 - F_c^2)^2]/\sum[w(F_o^2)^2]\}^{1/2}$.

After being stirred for 1 h, the solution was allowed to stand for 24 h before the solvent was removed in vacuo. The yellow solid was extracted into 150 mL of Et₂O, and this extract was filtered to remove Et₄NPF₆. Evaporation of the filtrate afforded a fine golden yellow powder. Yield: 350 mg (66%). ¹H NMR (THF-d_8): δ 1.628 (s, 15H), 1.652 (s, 30H), 2.004 (s, 30H), 2.008 (s, 15H), and 2.046 (s, 15H). ¹³³Cs NMR (THF): δ 92.0 (s). IR (MeCN, cm⁻¹): ν_{CN} = 2158, 2142, 2124, and 2121. ESI-MS: m/z = 2107 ([M⁺]). Anal. Calcd for $C_{82}H_{95}$-CsN₁₂Rh₄Ru₃: C, 46.78; H, 5.02; N, 7.98. Found: C, 45.75; H, 5.20; N, 7.53. Crystals of **Cs⊂Rh₄Ru₃** were obtained by cooling a saturated THF solution of **Cs⊂Rh₄Ru₃**.

NH₄⊂[Cp*Rh(CN)₃]₄[Cp*Ru]₃ (NH₄⊂Rh₄Ru₃). A solution of 611 mg (1.211 mmol) of [Cp*Ru(NCMe)₃]PF₆ in 50 mL of MeCN was added dropwise to a solution of 66 mg (0.404 mmol) of NH₄PF₆ and 750 mg (1.615 mmol) of Et₄N[Cp*Rh(CN)₃] in 325 mL of MeCN. After being stirred for 1 h, the solution was allowed to stand for 24 h before the solvent was removed in vacuo. The yellow solid was extracted into 150 mL of Et₂O, and this extract was filtered to remove Et₄NPF₆. Evaporation of the filtrate afforded a fine golden yellow powder. Yield: 610 mg (76%). IR (MeCN, cm⁻¹): ν_{CN} = 2119, 2147, 2160; ν_{NH} = 3270 (sh), 3246, and 3196. ¹H NMR (THF): δ 1.63 (s, 15H), 1.66 (s, 30H), 2.00 (s), 2.01 (s, 45H), 2.04 (s, 15H), and 5.40 (m, 4H). ESI-MS: m/z = 1992 ([M⁺]). Anal. Calcd for $C_{82}H_{99}N_{13}Rh_4$-Ru₃: C, 49.45; H, 5.52; N, 9.14. Found: C, 49.53; H, 5.43; N, 8.88. Crystals of **NH₄⊂Rh₄Ru₃** were obtained by layering a THF solution of **NH₄⊂Rh₄Ru₃** with MeCN and hexane.

Cage Formation Monitored by ESI-MS. A solution of 49 mg (0.097 mmol) of [Cp*Ru(NCMe)₃]PF₆ in 10 mL of MeCN was added dropwise to a solution of 9 mg (0.032 mmol) of CsOTf and 60 mg (0.129 mmol) of Et₄N[Cp*Rh(CN)₃] in 10 mL of MeCN. The reaction was monitored by negative and positive mode ESI-MS at 1, 4, 11, and 24 h. ESI-MS samples were diluted with MeCN to give 10^{-11} mol/μL concentrations. Experiments were run in duplicate with a MS/MS experiment following each interval. In these experiments, the cone voltage was varied between 25 and 35 V with no effect on the ion abundances.

¹³³Cs NMR Measurements. Measurements were conducted at 66 MHz on a Varian Unity INOVA 600 spectrometer with the following settings: delay time of 2 s, pulse width of 15 μs, and acquisition times were typically 2.0 s. Samples were approximately 5 mM (MeCN or THF solvent) in 5 mm tubes. Chemical shifts were referenced to a 1 M CsOTf solution of MeCN at δ34.362.

The ¹³³Cs MAS NMR measurements were conducted at 66 MHz on a Varian Unity INOVA 750 spectrometer with the following settings:

delay time of 1 s, pulse width of 8.3 μs, and acquisition times were typically 0.5 s.

Conversion of NH₄⊂Rh₄Ru₃ into Cs⊂Rh₄Ru₃. A solution of 7 mg (0.025 mmol) of CsOTf in 3 mL of CD₃CN was added to a solution of 50 mg (0.025 mmol) of **NH₄⊂Rh₄Ru₃** in 3 mL of CD₃CN, which was immediately (25 min) monitored by ¹³³Cs NMR, showing a single signal at δ 88. A similar experiment was performed by ¹H NMR.

Competition Experiment of BC6B versus NH₄⊂[Cp*Rh(CN)₃]₄-[Cp*Ru]₃. A solution of 7 mg (0.026 mmol) of CsOTf and 24 mg (0.026 mmol) of calix[4]arene-bis(benzocrown-6) in 12 mL of CD₃-CN was allowed to stand for 24 h. The solution was then monitored by ¹³³Cs NMR, which revealed one signal at −17 ppm and no free cesium at 34 ppm. A solution of 52 mg (0.026 mmol) of **NH₄⊂Rh₄Ru₃** in 3 mL of CD₃CN was added to the initial solution of CsOTf and calix[4]arene-bis(benzocrown-6). The solution was immediately monitored (approximately 1 h) by ¹³³Cs NMR, which revealed one signal at δ 88. A similar experiment was run in THF solvent, which yielded a similar result. The calix[4]arene-bis(benzocrown-6) ligand was obtained from ACROS.

Crystallography. Crystals were mounted on thin glass fibers using Paratone-N oil (Exxon) before being transferred to a Siemens Platform/CCD automated diffractometer for data collection. Data processing was performed with SAINT PLUS version 6.22. Structures were solved using direct methods and refined using full matrix least squares on F^2 using the program Bruker SHELXTL version 6.10. Hydrogen atoms were fixed in idealized positions with thermal parameters 1.5× those of the attached carbon atoms. The data were corrected for absorption on the basis of Ψ-scans. Specific details for each crystal are given in Table 2. Full crystallographic details have been deposited with the Cambridge Crystallographic Data Center.

Supporting Information Available: Crystallographic data (CIF format) including experimental details and complete tables of bond distances and angles, atomic coordinates, and anisotropic displacement parameters (PDF). This material is available free of charge via the Internet at http://pubs.acs.org.

JA035253H